Reliability of High Mobility InGaAs Channel n-MOSFETs under BTI Stress

Ming-Fu Li, Guangfan Jiao, Yaodong Hu, Yi Xuan, Daming Huang, and Peide D. Ye

Abstract- **The reliability performance of $In_xGa_{1-x}As$ n-MOSFETs with Al_2O_3 gate dielectric under PBTI stress is investigated. The following new phenomena are demonstrated: (1) There are high densities of fast interface traps N_{it} and slow oxide border traps N_{SOX} near the interface between InGaAs and Al_2O_3. The border traps are more fragile under stress and therefore the stress mainly induces border traps. (2) The stress induced border traps consist of permanent acceptor traps and recoverable donor traps. The acceptor trap energy density $\Delta D_{SOX}^{Acceptor}(E)$ is mainly distributed above the conduction band edge E_c of InGaAs with a tail extending to the mid-gap, while the donor trap energy density $\Delta D_{SOX}^{Donor}(E)$ has a large distribution inside the InGaAs energy gap with a tail extending to the conduction band. (3) Flicker noise variation after stress and its correlation to the acceptor and donor trap generation and recovery are demonstrated. (4) The recoverable donor traps induce the sub-threshold slope and off-current degradation in the stress phase and recover in the recovery phase, and also induce continuous degradation of on-current in the recovery phase. The permanent acceptor traps induce the transconductance and on-current degradation. The long term device life-time is mainly determined by the generation rate of the acceptor traps. (5) Comprehensive comparison between the Si and InGaAs MOSFETs degradation behaviors under BTI stress are presented. The physical recovery of donor oxide traps in dielectric in InGaAs/Al_2O_3 has never been observed in Si MOS structure, deserving special attention and further investigation.**

Index Terms—**InGaAs, n-MOSFETs, reliability, bias temperature instability (BTI), border traps.**

I. INTRODUCTION

InGaAs is a promising candidate among various high mobility channel materials for future n-MOSFETs for low voltage low power applications [1]-[10]. In this paper, we would summarize and elaborate our recent investigations [11], [12] regarding the impact of interface traps and border traps in the InGaAs/Al_2O_3 interface to the reliability performance of the n-MOSFETs under the positive-bias temperature instability (PBTI) stress.

$In_xGa_{1-x}As$ n-MOSFETs with $x = 0.53$ and 0.65 are used with the device structure shown in Fig.1. The fabrication processes of these devices were illustrated in [3]. The FETs have channel width *100 μm* and channel length *2 – 40 μm*, ALD grown Al_2O_3 gate dielectric with physical thickness of *8 nm*, and Ni/Au metal gate. P-type channel doping is about $1 – 2 \times 10^{17}\ cm^{-3}$.

D.C current-voltage (I_s-V_g), charge pumping (CP), fast pulsed I-V measurement (FPM), and flicker (*1/f*) noise measurements are carried out to characterize the degradation of n-MOSFETs under PBTI stress. Agilent 4156C parameter analyzer, pulse generator 81110A, and Cascade probe station are used for D.C I_s-V_g and CP measurements. In the I_s-V_g measurements, V_d is set to *50 mV*, while source and substrate are grounded. I_s rather than I_d is measured to avoid the drain-substrate junction reverse biased leakage interference. In the CP measurements [13], the source, drain, and substrate are all grounded. The CP currents I_{cp} are measured from the source/drain ($I_{s/d}$) and from the substrate (I_{sub}) with the similar results, indicating that the geometric component [13] due to electron-hole recombination in the channel is small and can be ignored. Comparing with I_{sub}, $I_{s/d}$ has smaller noise and therefore is used to characterize I_{CP}. During the PBTI stress phase, gate stress voltage $V_g = 3.0\ V$, while $V_s = V_d = V_b = 0\ V$. During the recovery phase, all the electrodes are grounded. The flicker noise measurements are conducted by SR570 low noise amplifier and Agilent 35670A spectrum analyzer. All measurements are taken at room temperature.

For the fresh transistors used in this work, the threshold voltage V_{th} is in the range of $+(0.1 \sim 0.2)V$ for the $x = 0.53$ FETs and $-(0.1 \sim 0.2)V$ for $x = 0.65$ FETs. The sub-threshold swing SS is around *130 meV/decade* for $x = 0.53$ FETs and *160meV/decade* for $x = 0.65$ FETs. Other electrical performance information can be found in [3].

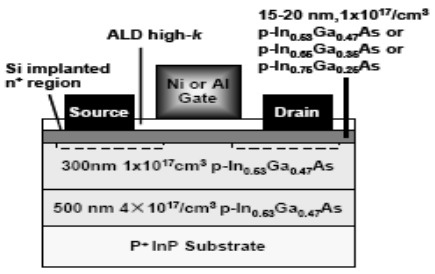

Fig.1 The structure of the planar inversion mode $In_xGa_{1-x}As$ n-MOSFET with ALD Al_2O_3 gate dielectric [3]

Ming-Fu Li, Guangfan Jiao, Yaodong Hu and Daming Huang are with the State Key Lab ASIC and System, Department of Microelectronics, Fudan University, Shanghai 201203, China. Email: mfli@fudan.edu.cn

Yi Xuan and Peide D.Ye are with school of Electrical and Computer Engineering and Birck Nanotechnology Center, Purdue University, West Lafayette, IN 47907, USA

This work in Fudan University is supported by National Natural Science Foundation of China project # 60936005, and the Micro/Nano-electronics Science and Technology Platform of Fudan University. This work in Purdue University is supported by NSF and the SRC FCRP MSD Focus Center.

In this paper, we mainly focus on the new phenomena under BTI stress in the InGaAs n-MOSFETs and compare to the traditional Si MOSFETs with SiON or high-k gate dielectric [14-20].

II. TRAPS GENERATION UNDER BTI STRESS - FAST INTERFACE TRAPS OR SLOW OXIDE BORDER TRAPS ?

Fig. 2 shows the charge pumping (CP) spectra for the $In_xGa_{1-x}As$ n-MOSFET during the PBTI stress phase and the following recovery phase, indicating generation of interface traps ΔN_t in the stress phase and partial recovery in the recovery phase. Fig.2(d) shows the time evolution of the CP currents I_{cp} and the areal density of the stress induced interface traps ΔN_t. From the I_{cp} of the fresh device, the process induced interface trap density N_t^0 is derived to be about $9 \times 10^{12}\ cm^{-2}$, very high comparing to $10^{10}\ cm^{-2}$ for a good quality Si MOSFETs. The stress-induced interface trap density $\Delta N_t = N_t - N_t^0$ is only about $1.3 \times 10^{11}\ cm^{-2}$ after *500 s* stress. The inset of Fig. 2(d) illustrates that the time evolution of ΔN_t in the stress phase shows a power law $\Delta N_t \propto t^n$ with index $n = 0.22$, close to the index n of Si/SiON p-MOSFET under negative BTI (NBTI) stress with similar CP measurement at room temperature [17]. On the other hand, N_t decreases in the recovery phase.

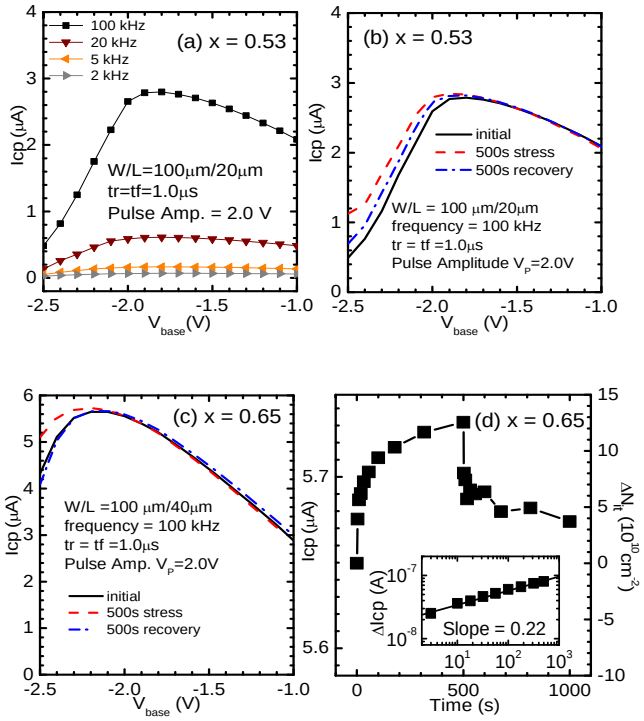

Fig.2. (a). CP current I_{cp} for the $In_{0.53}Ga_{0.47}As$ n-MOSFET fresh device measured at different frequencies. When V_{base} scans to *-1.85V*, the bottom level of CP pulse is at *-1.85V* and the FET is under accumulation, while the top level of CP pulse is at *+0.15V* (CP pulse amplitude *2V*), exceeding the V_{th} *=+0.1V* and the FET is under inversion. The CP current has a peak accordingly; (b). same FET measured by *f=100kHz* at the different states; (c) same as (b), however for $In_{0.65}Ga_{0.35}As$ FET. The interface trap area density is estimated by $N_t = I_{cp}/(fqA_G)$, A_G is the gate area. From the I_{CP} peak of the fresh device, $N_{it}^0 \approx 9 \times 10^{12}\ cm^{-2}$. (d) The time evolution of I_{cp} (left coordinate) and ΔN_t (right coordinate) in the stress phase (0 - 500 s) and recovery phase (500 - 1000 s). Inset: The time evolution of ΔI_{cp} in the stress phase plotted in log scale.

Fig. 3 shows the D.C I_s-V_g curves measured for the fresh device before stress (initial state, I lines), after 500 s PBTI stress (S lines), and with additional 500 s recovery (R lines) for $x = 0.65$ and 0.53 devices respectively.

Notice that by *f=100kHz* CP measurements showed in Fig.2, the stress induced interface trap area density ΔN_t is only $1.3 \times 10^{11}\ cm^{-2}$, comparing with the process induced interface trap area density N_t^0 ($\approx 9 \times 10^{12}\ cm^{-2}$) of the fresh device. However by I_s-V_g measurements showed in Fig. 3, ΔN_t is very large, $> 10^{12}\ cm^{-2}$ estimated by the gate voltage shift ΔV_g in the sub-threshold (SS) region by $\Delta N_{it} = (C_{OX}/q)\Delta V_g$, ($C_{OX}$ is the gate oxide capacitance) [21], as explained in more details in section IV. To resolve this issue, two additional experiments have been conducted.

Fig. 4 shows the frequency (f) dependence of N_t^0 and ΔN_t estimated by CP experiments. The f dependent CP results indicate that CP detected N_t has two trap components. The conventional fast interface trap component N_{it} which has f independent CP current component in the measured frequency range. The near interface slow oxide border trap component N_{SOX}, which has CP current decreasing with increasing f [22],[23], since when increasing f, the exchange of electrons between the slow border traps and the channel can not follow the rapid change of surface potential under CP measurement. The measured CP data in Fig.4 shows that when f is decreased from *100 kHz* to *1 kHz*, the process induced N_t^0 increases slightly while the stress induced ΔN_t increases more significantly. **This indicates that the process induced N_t^0 mainly includes the conventional fast interface traps N_{it}, while the stress induced ΔN_t mainly consists of the slow oxide border traps ΔN_{SOX}. The later is seriously underestimated by CP measurements. In other words, the border traps N_{SOX} are more fragile under stress than the**

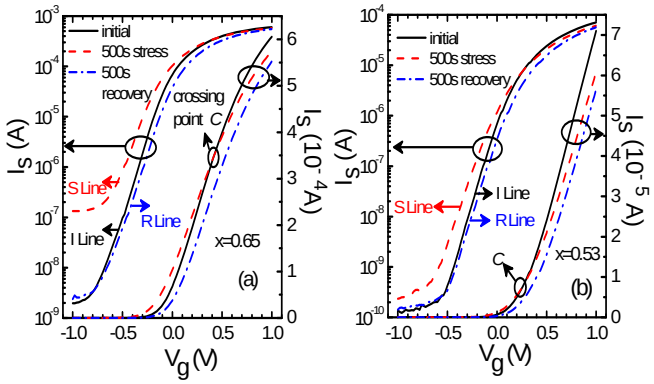

Fig. 3 I_s-V_g curves for the fresh $In_xGa_{1-x}As$ nMOSFET (solid lines, denoted by I lines), after 500 s PBTI stress (V_g = 3.0 V) (dashed lines, denoted by S lines), and then after 500 s recovery (V_g = 0 V) (dashed-dot lines, denoted by R lines). $V_d = 50\ mV$. (a) $x = 0.65$, $W/L = 100\ \mu m/4\ \mu m$. (b) $x = 0.53$, $W/L = 100\ \mu m/8\ \mu m$. Comparing S lines with I lines, the V_g shift ΔV_g at constant current I_s is negative in the sub-threshold region and is positive at high I_s in the on-current region. A crossing point C is defined at $\Delta V_g = 0$.

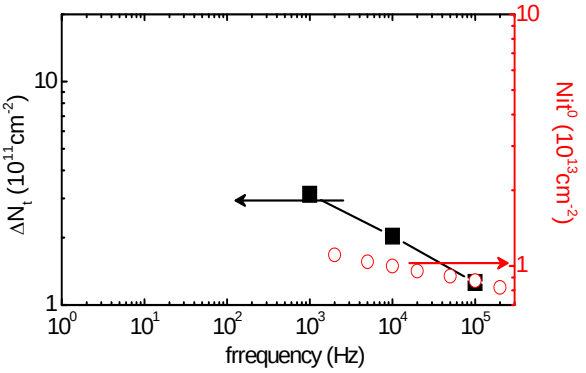

Fig.4. Frequency dependence of N_t^0 (open circle symbols, scaled by the right coordinate) and ΔN_t (solid square symbols, scaled by the left coordinate) estimated from CP experiments with the CP pulse with the constant rising and falling rates dV/dt = 2 V/μs. N_t^0 or ΔN_t is estimated by $I_{cp}/(fqA_G)$

conventional fast interface traps N_{it}. By extrapolating the data in Fig. 4 to frequency of *1 Hz*, the magnitude of ΔN_t could exceed 10^{12} cm^{-2}, in consistent with the results estimated by the D.C I_s-V_g measurements in the similar time zone of measurements. Using the method in [22], the volume density of the stress induced border traps is estimated to be ~ 5×10^{18} cm^{-3}.

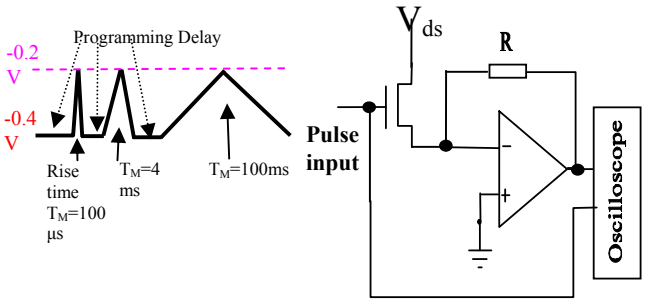

Fig.5. Left : The pulse waveform for the FPM measurement . Each measurement procedure consists of three sequential pulses with T_M=*100µs, 4ms* and *100 ms* respectively. The pulse is used to input to the circuit shown in the right side in Fig.5 [11,25].

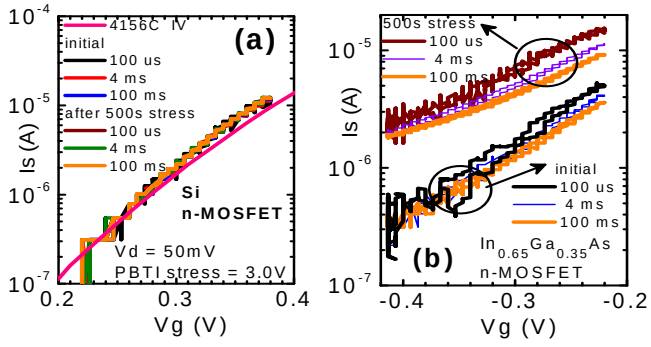

Fig.6. I_s-V_g curves in the sub-threshold region measured by the FPM method. **(a)** For Si nMOSFET. all curves measured by different T_M coincide completely, implying no error introduced by the FPM method. Small deviation from the curve measured by Agilent 4156C is due to scaling difference between 4156C and the amplifier used in FPM. **(b)** For fresh (initial) $In_{0.65}Ga_{0.35}As$ nMOSFET and after 500s PBTI stress. The curves measured by faster T_M has smaller sub-threshold swing S and larger ΔV, indicating existence of slow donor oxide traps.

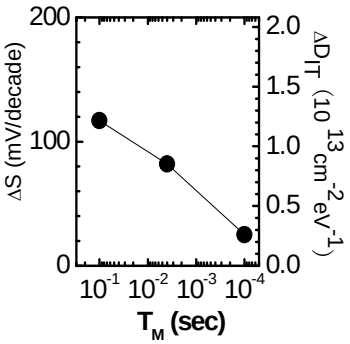

Fig.7. Degradation of sub-threshold swing ΔS after 500s PBTI stress (left coordinate) , extracted from the data in Fig.6(b). The generated slow oxide trap energy density $\Delta D_{SOX}=[C_{OX}/(qkTln10)]\Delta S$ [21] is also plotted (right coordinate). ΔD_{SOX} is seriously underestimated when T_M is reduced, indicating domination of slow donor oxide traps.

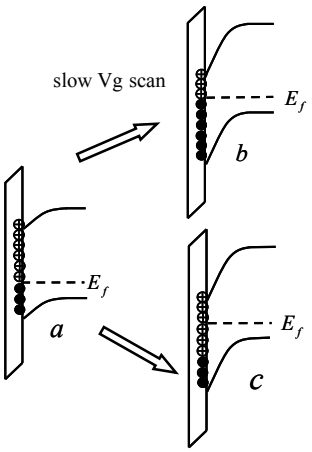

Fig.8. Surface potential band diagrams of $In_{0.65}Ga_{0.35}As$ n-MOSTEF used to explain the results of Figs. 6(b) and 7. **(a)** Surface potential for V_g= *- 0.4V,* **(b)** Surface potential for V_g= *- 0.2V* by slow V_g scan from *-0.4V*. Slow donor traps can response to capture electrons from the channel to reduce the positive charge, causing smaller ΔV_g and larger ΔS. **(c)** Same as (b) however for fast scan of V_g, slow donor traps can not response, no change of positive charge, causing larger ΔV_g and smaller ΔS.

The second additional experiment to support this argument is to use the fast pulsed I_s-V_g measurement (FPM) we have developed [24],[25], however extend to the SS region with lower detected current level and more challenging, as shown in Fig.5. Three I_s-V_g curves are measured by FPM in sequence using different measurement times T_M in 10^{-1}-10^{-4} s time zone. Reducing T_M should reduce the sub-threshold slope (S) degradation if the slow border traps ΔN_{SOX} can not follow the fast surface potential change in the FPM measurement. This is demonstrated in Figs. 6-8. **Combining Fig. 4 and Fig. 7 gives very strong support of domination of slow oxide border traps ΔN_{SOX} in the stress induced traps ΔN_t.**

III. DONOR OR ACCEPTOR TRAPS ? A UNIFIED BORDER TRAP MODEL

In the Fig.3, by comparing the I and S lines, ΔV_g extracted at low I_s (SS region) is negative after stress, accompanied by a degradation in sub-threshold swing S. The time evolutions of ΔV_g and ΔS are shown in Figs.9 and 10(a). ΔV_g extracted at high I_s ("on-current" region) is positive after stress, accompanied by a degradation in transconductance G_m, as shown in Figs.3, 9, and 10(b). There is a crossing point between the I and S lines in Fig.3, denoted by C at which ΔV_g = 0. On the other hand, by comparing the I and R lines in Fig.3, ΔV_g extracted at low I_s in the SS region is positive, with a degradation in S, as also shown in Figs. 9 and 10(a) at *t=1000s*. The most strange thing is that,

at high I_s, ΔV_g further degrade (increase) when the stress is released in the recovery phase as shown in Fig.3 S and R lines, and in Fig.9, and it saturates gradually towards a constant.

Interestingly, these results are totally different from the BTI degradation in the Si MOSFETs. For Si MOSFET with SiON gate dielectric, BTI stress induces dominant donor interface traps [26,27], and very small amount of acceptor interface traps [28]. When using DC current measurement, the donor interface traps induce negative V_g shift in the p-MOSFET under negative BTI stress [17,18,26]. The small amount of acceptor interface traps induce very small positive V_g shift in the n-MOSFET under PBTI stress [28] while donor interface traps keep neutral under inversion surface. For Si n-MOSFET with high-k gate dielectric HfO_2, I_s-V_g curve sustains positive shift in the PBTI stress phase and partially recover in the recovery phase [24]. The shift of *I-V* curve is due to trapping and de-trapping of the process induced pre-existing traps in the dielectric [24, 29-31].

To interpret the experimental results in Figs.3,9 and 10, the following picture in Fig.11 to distinguish the donor or acceptor traps is useful [32]. Comparing I and S lines in Fig.3 and Fig.11, it is clear that the stress induces donor border traps in the stress phase, responsible for the negative ΔV_g and the degradation of S in the SS region in Fig.3. The stress also induces acceptor interface traps or the fixed charge, responsible for the positive ΔV_g in the high I_s region and the degradation of transconductance G_m as shown in Figs. 3, 9, and 10(b).

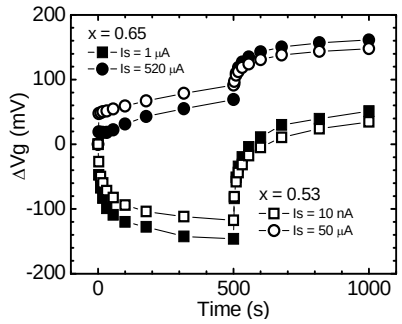

Fig. 9. Time evolution of ΔV_g in the SS region and in the on-current region in stress (0-500s) and recovery (500-1000s) phases, extracted from DC I_s-V_g curves shown in Fig.3. Note the strange phenomena that (1) ΔV_g in the on-current region continuously degrade (increases) in the recovery phase, (2) ΔV_g in the SS region turns to positive at the end of the recovery phase.

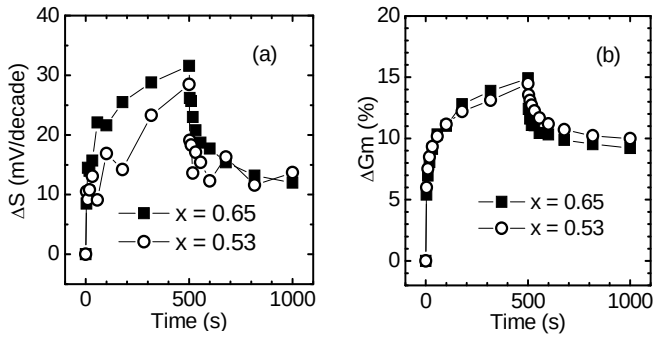

Fig. 10. Time evolution of (a) the ΔS extracted at I_s = 5.0 μA for x = 0.65 device and extracted at I_s = 10 nA for x = 0.53 device. (b) Time evolution of the degradation in peak transconductance.

Comparing the R lines with I lines in Fig.3 in the SS region, there are two possible cases to interpret the lines after the recovery phase. (1) There are recoverable donor traps and permanent acceptor traps. At the end of recoverable phase, donor traps are recovered and only acceptor traps exist, which can explain the positive ΔV_g and the S degradation (see the difference between the I and R lines in Fig.3 and compare it with Fig. 11(b)). (2) There are recoverable donor traps and fixed negative oxide charge. In the case (2), the R lines in Fig.3 are the combined effect of the fixed negative oxide charge and the residual donor traps. The fixed negative charge induces parallel positive shift in the I_s-V_g curve. The residual donor traps at the end of the recoverable phase induce the degradation of S and the negative ΔV_g. If it is the case (2), the residual donor traps must have high enough density to compensate the positive shift induced by the fixed negative charge. As a result, the net ΔV_g is close to zero only when I_s is very low (4×10^{-9} A for x = 0.65 devices and 3×10^{-10} A for x = 0.53 devices), as shown in Fig. 3. The case (2) should be ruled out because the recovered off-current I_s^{off} (discussed in Section V, Fig.15) reveals that the stress induced donor traps almost completely recovered in the end of the recovery phase. These results are in conflict with the case (2), but in supporting the case (1).

By the above arguments, a unified border trap model can be established to explain perfectly every details of all experimental results. As explained in Fig.12, the stress induces slow border traps with density ΔN_{SOX} include recoverable donor traps with energy density $\Delta D_{SOX}^{Donor}(E)$ and permanent acceptor traps with energy density $\Delta D_{SOX}^{Acceptor}(E)$. The recoverable $\Delta D_{SOX}^{Donor}(E)$ traps is not only distributed within the InGaAs energy gap but

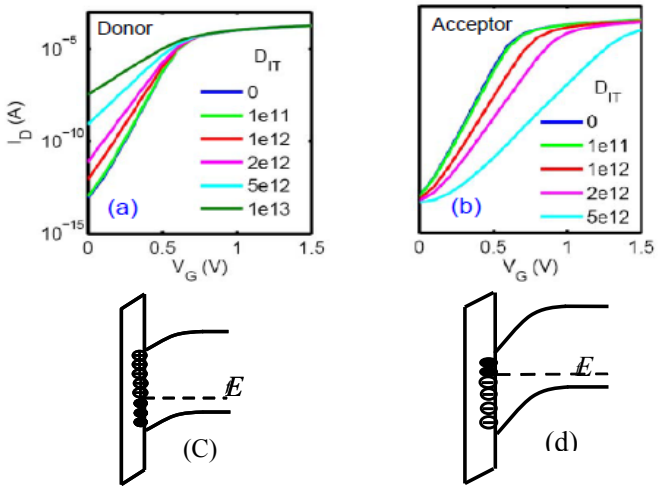

Fig.11. (a) donor traps at the interface induce negative V_g shift of the *I-V* curves, larger shift with lower I_s current level, (b) Acceptor traps at the interface induce positive shift of the *I-V* curves, larger shift with higher I_s current level.(courtesy of M.A.Alam [32]). This can be understood by the MOS band diagrams in (c) (d). Higher I_s level corresponds to stronger inversion with deeper band bending, inducing lower positive interface charge area density for donor traps (c) , causing smaller V_g shift as shown in (a); or higher negative interface charge area density for acceptor traps (d), casing larger V_g shift as shown in (b). Both acceptor and donor traps give rise degradation of S.

also extended to the conduction band. The donor traps within the energy gap induce the negative ΔV_g and the S degradation in the stress phase and the recovery in the SS region during the recovery phase (Figs. 3, 9, and 10(a)). The donor traps in the conduction band induce the strange phenomena of continuous increase of positive ΔV_g in the recovery phase (Figs. 3 and 9). On the other hand, the permanent acceptor traps energy density $\Delta D_{SOX}{}^{Acceptor}(E)$ is mainly distributed in the conduction band with a tail extending to the energy gap. The acceptor traps in the conduction band induce the positive ΔV_g and the degradation in G_m in the high I_s region in the stress phase (Figs. 3, 9, and 10(b)). The acceptor traps in the energy gap result in the positive ΔV_g and the small S degradation in the SS region at the end of recovery phase (Figs. 3, 9, and 10(a)). Finally, all the border traps are seriously underestimated by the CP measurements when they cannot follow the fast change of the surface potential during the CP measurements.

It should be emphasized that the properties of the oxide border traps in the InGaAs/Al_2O_3 is totally different from the oxide traps in SiON or high-k dielectrics in the Si MOSFETs. In Si MOSFETs, many works demonstrated that the oxide traps are mainly pre-existing traps during transistor fabrication process in the gate dielectric of SiON [19],[33]or high-k [24],[29]-[31]. The degradation and recovery reflected in the I-V curves are mainly trapping and de-trapping of electrons (or holes) in the pre-existing traps in the stress phase and recovery phase. However in the InGaAs/Al_2O_3 case, the oxide traps are generated in the stress phase. The trapping and de-trapping are reflected in the degradation of S, the transconductance, and the off current (as shown in section V) in the I-V curves. Particularly, donor oxide traps physically recover in the recovery phase. This is very unique and has never been observed by the Si MOSFETs community so far. The origin and physical mechanism of generation and recovery of donor oxide border traps in the InGaAs/Al_2O_3 interface deserve special attention and investigation in the future.

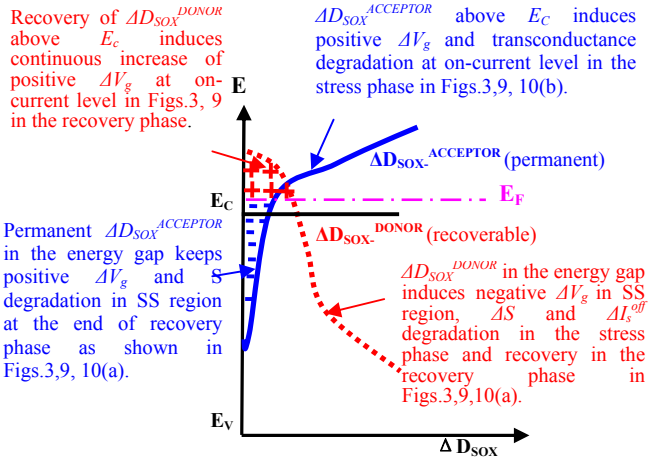

Fig. 12. Stress induced oxide border trap density $\Delta D_{SOX}(E)$ which consists of permanent acceptor traps $\Delta D_{SOX}{}^{Acceptor}$ (solid line) and recoverable donor traps $\Delta D_{SOX}{}^{Donor}$ (dashed line). During the I_s-V_g measurement, when E_F is moved to a level that the positive donor trap charge is equal to the negative acceptor trap charge, corresponding to the crossing point C at which $\Delta V_g = 0$ in Fig. 3.

IV. EXTRACTIONS OF BORDER TRAP ENERGY DENSITIES FROM EXPERIMENTS

We can use the I_s-V_g curves in Fig. 3 to extract the energy distribution of stress induced border traps based on the following assumptions for the trap model described in section III. (1) At the end of 500 s stress, there are both stress induced donor traps and acceptor traps in the devices. (2) At the end of 500 s recovery, the stress induced donor traps fully recover (see Sec. V Fig.15) while the acceptor traps are permanent. The extraction procedure is as follows.

The first step: ΔV_g is extracted from the I (initial) and R (after 500s recovery) lines as a function of I_s for all the current range shown in Fig.3. The result is denoted by $\Delta V_g{}^{IR}(I_s)$. Since only the acceptor traps remain after 500 s recovery, the density $\Delta N^-_{SOX}{}^{Acceptor}(I_s)$ of negatively charged acceptor traps as a function of I_s can be obtained by [21]

$$\Delta N^-_{SOX}{}^{Acceptor}(I_s) = (C_{OX}/q)\Delta V_g{}^{IR}(I_s) \quad (1)$$

where C_{OX} is the gate oxide capacitance per unit area and is 10^{-6} F/cm^2 estimated by 8 nm Al_2O_3 gate dielectric. On the other hand, the density difference of negatively charged acceptor traps and positively charged donor traps, $\Delta N^-_{SOX}{}^{Acceptor}(I_s)$ - $\Delta N^+_{SOX}{}^{Donor}(I_s)$, can be extracted from the I and S (after 500s stress) lines, shown in Fig. 3, by

$$\Delta N^-_{SOX}{}^{Acceptor}(I_s) - \Delta N^+_{SOX}{}^{Donor}(I_s) = (C_{OX}/q)\Delta V_g{}^{IS}(I_s) \quad (2)$$

where $\Delta V_g{}^{IS}(I_s)$ is the V_g difference between the S and I lines at the same I_s. From Eqs. (1) and (2), the density of positively charged donor traps can be obtained from

$$\Delta N^+_{SOX}{}^{Donor}(I_s) = (C_{OX}/q)\Delta V_g{}^{IR}(I_s) - (C_{OX}/q)\Delta V_g{}^{IS}(I_s) \quad (3)$$

The second step: the surface potential ψ_s and the energy difference $E = E_F - E_V$ at the interface as a function of I_s can be calculated by SILVACO Atlas simulation tool for $In_xGa_{1-x}As$ nMOSFETs. The device structures for simulations are the same as real devices shown in Fig.1. From these simulations, the relationship between I_s and the corresponding $E(I_s)$ are obtained. Combining (1), (3), and $E(I_s)$, we obtain $\Delta N^+_{SOX}{}^{Donor}(E)$ and $\Delta N^-_{SOX}{}^{Acceptor}(E)$ as functions of energy E as shown in Fig.13.

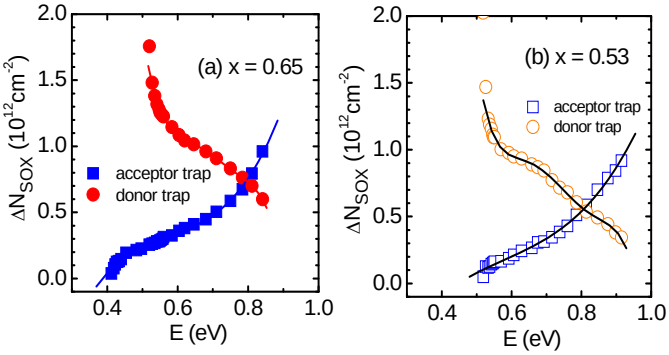

Fig.13. The charged donor and acceptor border trap area densities as a function of $E=E_F - E_V$ extracted from ΔV_g. The solid lines are least square fits by polynomials.

The energy distribution of donor and acceptor traps can be obtained from

$$\Delta D_{SOX}^{\ Donor}(E) = -\frac{d\Delta N^{+}_{\ SOX}{}^{Donor}}{dE} \quad (4)$$

$$\Delta D_{SOX}^{\ Acceptor}(E) = \frac{d\Delta N^{-}_{\ SOX}{}^{Acceptor}}{dE} \quad (5)$$

The results of Eqs. (4) and (5) are plotted in Fig. 14.

There are two possible error sources in obtaining the donor and acceptor trap densities using the above derivations. (1) The mobility degradation induced ΔV_g in the strong inversion region [26] has been overlooked. Therefore both the donor and acceptor trap densities may be overestimated, giving rise to distortions of the curves in the horizontal direction in Fig. 14 in the conduction band region. (2) The Atlas simulator for III-V MOSFETs simulation is not matured, and may introduce some error in $E(I_s)$ relation, giving rise to distortions of the curves in the vertical direction in Fig. 14. In spite of these distortions, the overall energy distributions of donor and acceptor traps demonstrated in Fig. 14 can explain all the experimental results. The stress induced donor traps have a large density in the energy gap and their distribution extends to the conduction band. The stress induced permanent acceptor traps are mainly distributed in the conduction band, with a tail extending to the mid-gap.

We can also extract the energy distributions of stress induced acceptor and donor traps from the ΔS in the SS region with the results in consistent with the results in Fig.14. The details are described in [12].

V. OFF-CURRENT DEGRADATION

In this section, we focus on the degradation under BTI stress and recovery in the recovery phase of the off-current in the range of V_g = -0.8 V to -1.0 V in Fig.3, denoted by I_s^{off}. Fig. 15 shows the time evolutions of the change of I_s^{off} (ΔI_s^{off}) at a constant gate voltage V_g = *-0.8 V* in the stress and recovery phases. ΔI_s^{off} increases with time in the stress phase and almost completely recovers in the recovery phase, implying that ΔI_s^{off} is related to the recoverable donor traps as discussed in section III.

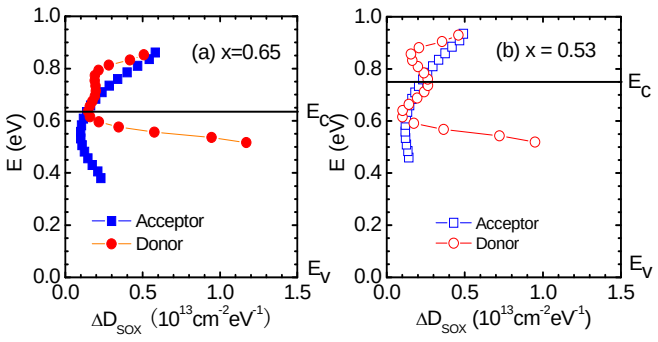

Fig. 14. The donor and acceptor trap energy densities extracted from Eqs. (4) and (5) for (a) $In_{0.65}Ga_{0.35}As$ and (b) $In_{0.53}Ga_{0.47}As$ n-MOSFETs.

As shown in Figs.3 and 15, both I_s^{off} and ΔI_s^{off} show large quantitative difference between x = 0.53 and 0.65 devices. For x = 0.53 device, the I_s^{off} is in the range of 10^{-10} *A* for the fresh device, and increases by a factor of 2 ~ 3 after *500 s* stress. For x = 0.65 device, the I_s^{off} is in the range of 10^{-9} *A* for the fresh device, and increases by two orders of magnitude after *500 s* stress. In order to clarify this issue, the ΔI_s^{off}-V_d curves measured after *500 s* stress and 500 s recovery were conducted. If ΔI_s^{off} is due to the change of surface potential pinning [34], [35], ΔI_s^{off} should be the diffusion current of minority carriers in the SS region satisfying the following equation [21]

$$\Delta I_s^{\ off} = A[1-\exp(-qV_d / kT)] \quad (6)$$

which saturates when $V_d > 3kT/q \approx 0.1$ *V*. As shown in Fig. 16(a), for x = 0.53, ΔI_s^{off} measured after 500 s stress satisfies equation (6). It implies that the degradation (recovery) of ΔI_s^{off} is due to the generation (recovery) of very large density of donor traps in the energy gap as shown in Figs.12 and 14, causing the change of surface potential pinning. However, as shown in Fig. 16(b) for x = 0.65 device, ΔI_s^{off} measured after 500 s stress does not satisfy equation (6). In that case, ΔI_s^{off} is likely due to the drift of electrons in a new surface conduction path across the source and drain, generated by high areal density of donor traps under stress, and therefore the I_s^{off}-V_d has a quasi- ohmic relationship. This surface conduction path could be due to the hopping conduction [36] between the neighboring donor traps induced by the stress.

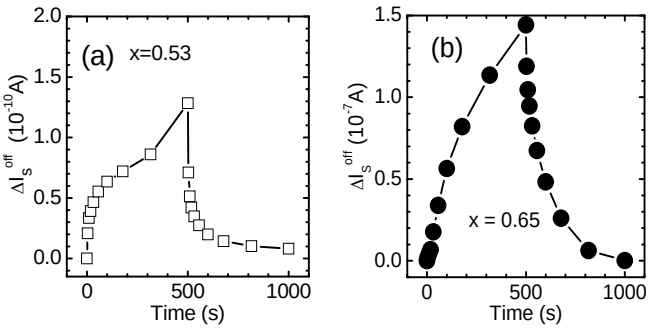

Fig. 15. Time evolutions of the ΔI_s^{off} at constant gate voltage V_g = -0.8 V in the stress (0-500s) and recovery (500-1000s) phases.

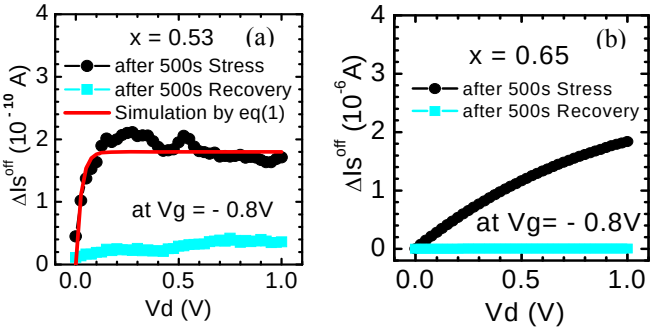

Fig. 16. (a) ΔI_s^{off}-V_d curves after 500 s PBTI stress and 500 s recovery for the x = 0.53 nMOSFET. The curve after stress satisfies eq(6), implying that ΔI_s^{off} under stress is due to generation of large amount of donor traps, causing change of surface potential pinning, (b) Same as (a) but for x = 0.65 FET. ΔI_s^{off}-V_d after 500 s PBTI stress does not satisfy equation (6).

VI. FLICKER NOISE CHRACTERIZATION

The flicker (*1/f*) noise measurement could be a powerful technique to characterize the oxide trap distribution in the gate dielectric of MOSFETs [37-39]. Since there are high densities of acceptor and donor oxide border traps in InGaAs nMOSFET generated under PBTI stress as described in the sections III-IV, *1/f* noise measurements should be useful to further understand the oxide trap properties as well as the MOSFET performance under stress. In this section, a preliminary *1/f* noise measurement result of $In_{0.53}Ga_{0.47}As$ n-MOSFETs under PBTI stress is presented.

Fig.17 shows the normalized noise power spectral densities $S(f)/I_d^2$ [37] versus frequency *f* for $In_{0.53}Ga_{0.47}As$ n-MOSFETs for the fresh device (spectrum I), right after 500s PBTI stress (spectrum S), and after *2000 s* recovery phase (spectrum R) respectively. Obvious correlations between the donor and acceptor border traps described in sections III-IV and the shape of the $S(f)/I_d^2$ spectra in Fig.17 are observed. (1) Since there are only acceptor oxide traps while all donor traps are almost completely recovered after the *2000 s* recovery phase as

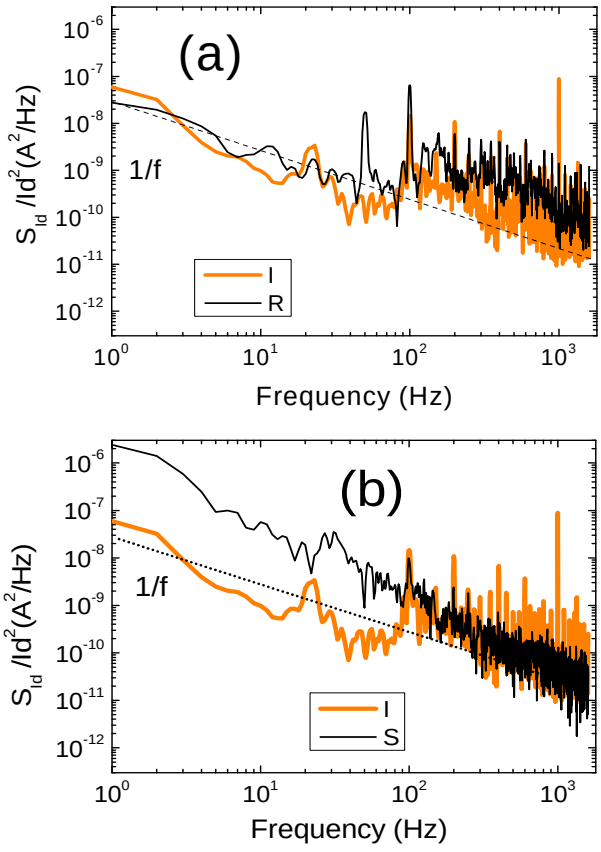

Fig.17 The normalized flicker noise power spectral densities $S(f)/I_d^2$ of $In_{0.53}Ga_{0.47}As/Al_2O_3$ n-MOSFET, measured at $V_g - V_{th} = 0.1V$, $V_d = 0.1V$. (a) comparison of I spectrum for the fresh device with R spectrum after 500S PBTI stress ($V_g = 3V$) and subsequently after 2000 recovery phase ($V_g = 0V$). (b) comparison of I spectrum with S spectrum measured right after 500 s PBTI stress . The additional peaks at the frequencies of n×50Hz (n is integer) are due to 50Hz city electric power interference and should be ignored.

described in sections III-V, the difference between spectra I and R in Fig. 17(a) reflects the contribution of generated acceptor border tarps to the S(f) spectrum. It is observed that acceptor border traps mainly affect (increase) the flicker noise in the frequency range around and above *100Hz*. (2) Since there are both donor and acceptor border traps at the instance right after *500s* PBTI stress, the difference between spectra I and S in Fig.17(b) reflects the contribution of both donor and acceptor traps to the S(f) spectrum. The S spectrum has significant increase in the frequency range below *100Hz* comparing to the I spectrum. Combining Fig. 17(a) and (b), it indicates that donor traps mainly affect (increase) the spectrum below *100Hz*. More detailed and quantitative investigations of flicker noise measurements and their correlation to the donor and acceptor border traps for the InGaAs n-MOSFET will be published else where.

VII. EFFECTS OF BORDER TRAPS ON THE DEVICE PERFORMANCE AND LIFE TIME.

As described in sections III-V, the donor traps mainly induce the off-current degradation. However the trapping and de-trapping of the donor traps response very slowly and may not response in fast switching applications in logic circuits. In the analog applications in a class A amplifier, a constant DC bias is applied with a constant DC operating current and therefore the off-current is also not important. Particularly, the degradation induced by donor traps is recoverable when the stress is released. Therefore the degradation is not cumulative in many ac switching circuit applications and in daily turn-on turn-off system. On the other hand, the acceptor traps degrade the on-current and transconductance permanently and the degradations are cumulative. In the long term device life-time determination, acceptor traps generation rate is the key factor to be concerned.

VII. CONCLUTIONS

We have presented the charge pumping, D.C and fast pulsed I_s-V_g measurements results to investigate the degradations under PBTI stress for the $In_xGa_{1-x}As$ nMOSFETs with $x = 0.53$ and 0.65. The stress induced traps are mainly slow oxide border traps including two components: (1) The recoverable donor traps with energy density $\Delta D_{SOX}^{Donor}(E)$. It has a large distribution in the InGaAs energy gap, with a tail extending to the conduction band. It is responsible for the negative ΔV_g in the sub-threshold region, the *S* degradation, the I_s^{off} degradation of the I_s-V_g curve in the stress phase, and continuous degradation of positive ΔV_g in the on current region in the recovery phase. The donor taps are almost completely recovered in the recovery phase. (2) The permanent acceptor traps with energy density $\Delta D_{SOX}^{Acceptor}(E)$. It is mainly distributed in the conduction band of InGaAs with a tail extending to the mid-gap. It is responsible for the positive ΔV_g and transconductance degradation in the on current region of the I_s-V_g curve after stress. The flicker noise power spectra and their correlation to the donor and acceptor border traps are also

shown. The device life-time is mainly determined by the acceptor border trap generation rate under stress. The border traps generated in InGaAs/Al_2O_3 MOS devices are very different from the traps in Si MOS devices with SiON or high-k dielectrics, and deserve more comprehensive investigations in the future.

REFERENCES

[1] G. Dewey, B. Chu-Kung, R. Kotlyar, M. Metz, N. Mukherjee and M. Radosavljevic, "III-V Field effect transistors for future ultra-low power applications", in *VLSI Symp. Tech. Dig*., 2012, p.45.

[2] J. A. del Alamo, "Nanometre-scale electronics with III-V compound semiconductors," *Nature*, vol. 479, pp. 317-323, 2011.

[3] Y. Xuan, T. Shen, M. Xu, Y. Q. Wu, and P. D. Ye, "High-performance surface channel In-rich $In_{0.75}Ga_{0.25}As$ MOSFETs with ALD high-k as gate dielectric," in *IEDM Tech. Dig.,* 2008, p. 371; JJ.Gu, X.W.Wang, H.Wu, J.Shao, A.T.Neal, M.J.Manfra, R.G.Gordon and P.D.Ye,"20-80nm channel length InGaAs gate-all around nanowire MOSFETs with EOT=1.2nm and lowest S=63mV/dec", in *IEDM Tech. Dig.,* 2012, p. 633.

[4] J. Huang, N. Goel, H. Zhao, C. Y. Kang, K. S. Min, G. Bersuker, S. Oktyabrsky, C. K. Gaspe, M. B. Santos, P. Majhi, P. D. Kirsch, H. -H. Tseng, J. C. Lee, R. Jammy, "InGaAs MOSFET performance and reliability improvement by simultaneous reduction of oxide and interface charges in ALD (La)AlOx/ZrO2 stack," in *IEDM Tech. Dig.,* 2009, p. 335.

[5] S. H. Kim, M. Yokoyama, N. Taoka, R. Nakane, T. Yasuda, O. Ichikawa, N. Fukuhara, M. Hata, M. Takenaka, S. Takagi, "Sub-60nm deeply-scaled channel length extremely-thin body InGaAs-on-insulatoir MOSFETs on Si with Ni-InGaAs metal S/D and MOS interface buffer engineering", in *VLSI Symp. Tech. Dig.,* 2012, p.177.

[6] H.-C. Chin, M. Zhu, Z.-C. Lee, X. Liu, K.-M. Tan, H. K. Lee, L. Shi, L.-J. Tang, C.-H. Tung, G.-Q. Lo, L.-S. Tan, and Y.-C. Yeo, "A new silane-ammonia surface passivation technology for realizing inversion-type surface-channel GaAs n-MOSFET with 160 nm gate length and high-quality metal-gate/high-k dielectric stack," in *IEDM Tech. Dig.,* 2008, p. 383.

[7]M.Heyns *et al*., "Advancing CMOS beyond the Si roadmap with Ge and III/V devices", in *IEDM Tech. Dig.,* 2011, p. 299.

[8] M. Passlack, G. Doornbos, C. Wann, and Y.C. Sun, "Classification and benchmarking of III-V MOSFETs for CMOS", in *VLSI Symp. Tech. Dig.,* 2010, p. 155.

[9] Y. Sun, E.W. Kiewra, J.P.de Souza, J.J. Buchhignano, K.E. Fogel, D.K. Sadana and G.G. Shahidi, "Sclaing of InGaAs buried-channel MOSFETs", in *IEDM Tech. Dig.,* 2008, p. 367.

[10] H.J.Oh, J.Q.Lin, S.A.B.Suleiman, G.Q.Lo, D.L.Kwong, D.Z.Chi and S.J.Lee, "Thermally robust phosphorous nitride interface passivation for InGaAs self-aligned gate first n-MOSFET integrated with high-k dielectric", in *IEDM Tech. Dig.,* 2009, p. 339.

[11] G. F. Jiao, W. Cao, Y. Xuan, D. M. Huang, P. D. Ye, M. F. Li, "Positive bias temperature instability degradation of InGaAs n-MOSFETs with Al_2O_3 Gate Dielectric," in *IEDM, Tech. Dig.*, 2011, p. 606.

[12] G. F. Jiao, C.J.Yao, Y. Xuan, D. M. Huang, P. D. Ye, M. F. Li, "Experimental investigation of border trap generation in InGaAs nMOSFETs with Al_2O_3 gate dielectric under PBTI stress", *IEEE Trans. Electron Devices,* vol.59, no.6, pp.1661-1667, 2012.

[13] G. Groeseneken, H. E. Maes, N. Beltran, and R. F. D. Keersmaecker, "A reliable approach to Charge-Pumping measurements in MOS transistors," *IEEE Trans. on Electron Devices*, vol.31, no. 1, pp. 42-53, 1984.

[14]E.H. Nicollian and J.R. Brews, *MOS Physics and Technology*, Wiley, New York, pp.794-798, 1982.

[15] T.Grasser *et al.*, "Recent advances in understanding the bias temperature instability", in *IEDM Tech. Dig.,* 2010, p.82.

[16] S.Mahapatra, N.Goel, S.Desai, S.Gupta, B.Jose, S.Mukhopadhyay, K.Joshi, A.Jian, A.E.Eslam and M.A.Alam, "A comparative study of different physics-based NBTI models", *IEEE Trans. Electron Devices,* vol.60, no.3, pp.901-, 916, 2013.

[17] V.Huard, C.Parthasarathy, N.Rallet, C.Guerin, M.Mammase, D.Barge, C.Ouvrard, "New characterization and modeling approach for NBTI degradation from transistor to product level", in *IEDM Tech. Dig.,* 2007, p.797.

[18] G.Chen, M.F.Li, C.H.Ang, J.Z.Zhen, and D.L.kwong, "Dynamic NBTI of p-MOS transistors and its impact on MOSFET scaling", *IEEE Electron Device Lett.*, vol.23, pp.734-736, 2002.

[19] M.A. Alam and S. Mahapatra, "A comprehensive model of PMOS NBTI degradation", Microelectronics Reliability, vol.45, pp.71-81, 2005.

[20] S. Chakravarthi, A. T. Krishnan, V. Reddy, C. F. Machala and S. Krishnan, "A comprehensive framework for predictive modeling of negative bias temperature instability," in *Proc. Int. Reliab. Phys. Symp.*, 2004, p. 273.

[21] S. M. Sze, *Physics of semiconductor devices*, Wiley, New York, 1981.

[22] R. E. Paulson and M. H. White, "Theory and application of charge pumping for the characterization of Si-SiO2 interface and near-interface oxide traps," *IEEE Trans. on Electron Devices,* vol. 41, pp. 1213-2778, 1994.

[23] Y. Maneglia and D. Bauza, "Extraction of slow oxide trap concentration profiles in metal-oxide-semiconductor transistors usin the charge pumping method", *J. Appl. Phys*., vol.79, p. 4187-4192, 1996.

[24] C.Shen, M.F.Li, X/P/Wang, H.Y.Yu, Y.P.Feng, A.T.L.Lim, Y.C Yeo, D.S.H.Chan and D.L.Kwong, "Negative U traps in HfO_2 gate dielectrics and frequency dependence of dynamic BTI in MOSFETs", *IEDM Tech. Dig.,* 2004, p.733.

[25] M.F.Li, D.M.Huang, C.Shen, T.Yang, W.J.Liu and Z.Y.Liu, "Understand NBTI mechanism by developing novel measurement techniques", *IEEE Trans. Device Mater. Rel ,* vol.8, pp.62-71 , 2008.

[26] T.Grasser, P.J.Wagner, P.Hehenberger, W.Gos and B.Kaczer,"A rigorous study of measurement techniques for negative bias temperature instability", in *IEEE Trans. Device Mater. Rel ,* vol.8, pp.526-535 ,2008.

[27] J.P. Campbell, P.M. Lenahan, A.T. Krishnan, and S. Krishnan, " Location, structure, and density of states and structure of NBTI-induced defects in plasma-nitrided pMOSFETs", in *Proc. Int. Reliab. Phys. Symp.*, 2007, p. 503.

[28] Z.Y.Liu, D.M.Huang, W.J.Liu, C.C.Liao, L.F.Zhang, Z.H.Gan, Waisim Wong and Ming-Fu Li, "Comprehensive studies of BTI effects in CMOSFETs with SiON by new measurement techniques", in *Proc. Int. Reliab. Phys. Symp.*, 2008, p.733.

[29] G.Bersuker, J.H. Sim, C.S.Park, C.D.Young, S.Nadkami, R.Choi, and B.H.Lee, "Intrinsic threshold voltage instability of the HfO_2 NMOS transistors", in *Proc. Int. Reliab. Phys. Symp.*, 2006, p.179.

[30] A.Kerber, E.Cartier, L.Pantisano, M. Rosmeulen, R.Degraeve, T.Kauerauf, G.Groeseneken, H.E.Maes, U.Schwalke, "Characterization of the Vt-instabilitry in SiO_2/HfO_2 gate dielectrics", in *Proc. Int. Reliab. Phys. Symp.*, 2003, p.41.

[31] A. Neugroschel, G. Bersuker, R. Choi and B.H. Lee, " Effect of the interfacial SiO_2 layer in high-k HfO_2 gate stacks on NBTI" , in *IEEE Trans. Device Mater. Rel ,* vol.8, pp.47-61, 2008.

[32] D. Varghese, Y. Xuan, Y. Q. Wu, T. Shen, P. D. Ye, and M. A. Alam, "Multi-probe interface characterization of In0.65Ga0.35As/Al2O3 MOSFET," in *IEDM, Tech. Dig,* 2008, p. 379.

[33] T.Yang, M.F.Li, C.Shen, C.H.Ang, C.Zhu, Y.C.Yeo, G. Samudra, S.C.Rustagi, M.B.Yu, and D.L.Kwong, "Fast and slow dynamic NBTI components in p-MOSFET and SiON dielectric and their impact on device life time and circuit applications", in *VLSI Symp. Tech. Dig*., 2005, p.758.

[34] N. Wrachien, A. Cester, E. Zanoni, G. Meneghesso, Y. Q. Wu and P. D. Ye, "Degradation of III-V inversion-type enhancement-mode MOSFETs," in *Proc. Int. Reliab. Phys. Symp.,* 2010, p. 536.

[35] M. Passlack, "OFF-state current limits of narrow bandgap MOSFETs," *IEEE Trans. on Electron Devices*, vol. 53, pp. 2773-2778, 2006.

[36] N. F. Mott and E. A. Davis, Electronic processes in non-crystalline materials, Clarendon Press, 1979, p.32.

[37] M.J.Kerton and M.J.Uren, "Noise in solid state microstrictures: a new perspective on individual defecets, interface states and low –frequency(1/f) noise", *Advances in Physics*, vol.38, no.4, pp.367-468,1989.

[38] R.Jayaraman and C.G.Sodini," A 1/f noise technique to extract the oxide trap density near the conduction band edge of Si", *IEEE Trans. Electron Devices*, vol. 36, no.9, pp.1773-1782,1989.

[39] G.Kapila, N.Goyal, V.D.Maheta, C.Olsen, K.Ahmed and S.Mahapatra," A comprehensive study of flicker noise in plasma nitrided SiON p-MOSFETs:Process dependence of pre-exsisting and NBTI stress generated trap distribution profiles", in *IEDM Tech. Dig.,* 2008,p.103.